

Evidence for narrow $D_s^* (2640)$ meson

decaying to $D_s\eta$

A.Evdokimov,* A.Dolgolenko, M.Kubantsev,[†] I.Larin, and J.Russ[‡]

ITEP Moscow

B.Cheremushkinskaya 25 ,

Moscow, Russia 117259

(Dated: May 3, 2004)

Abstract

Using SELEX Pass1 data we have observed a new narrow peak in the $D_s\eta$ final state with a mass near $2640 \text{ MeV}/c^2$. A D_s sample is reconstructed from $D_s^+ \rightarrow K^-K^+\pi^+$ and $D_s^- \rightarrow K^-K^+\pi^-$ decays. An η sample is reconstructed from decays $\eta \rightarrow \gamma\gamma$ and $\eta \rightarrow \pi^+\pi^-\pi^0$ decays. We observed a peak of 54 ± 13 events at mass $2640 \pm 0.004 \text{ MeV}/c^2$ with width $11 \text{ MeV}/c^2$ of in the decay mode $D_s^* \rightarrow D_s(\eta \rightarrow \gamma\gamma)$ and a peak of 25 ± 7 events at mass $2649 \pm 0.006 \text{ MeV}/c^2$ with width $16 \text{ MeV}/c^2$ in the decay mode $D_s^* \rightarrow D_s(\eta \rightarrow \pi^-\pi^+\pi^0)$. As shown by Monte Carlo study these widths are compatible with experimental resolution. Statistical significance of the peaks is 7σ and 4σ correspondently. $D_s^*(2112) \rightarrow D_s\gamma$ and $D_s^*(2460) \rightarrow D_s\gamma$ are also observed. Some properties of the observed $D_s\eta$ state are presented.

Keywords:

*Electronic address: evdokim@fnal.gov

[†]Also at Physics Department, Northwestern Illinois University.

[‡]Physics Department, Carnegie-Mellon University.

I. INTRODUCTION

In 2003 two new states have been observed with charm and strangeness by Babar, Belle, CDF and CLEO. Despite the fact that SELEX statistic for D_s mesons is lower than in these experiments, it is worth trying to look for decays with charm and strangeness involving photons in final state reconstructed in SELEX Photon detectors.

II. D_s RECONSTRUCTION.

The program used for reconstruction of charged particle tracks is a SOAP standard pass2.tseg. The data used are from a D_s meson strip created by Ilia Larine from pass1 meson output stream using information fn781: /anal01/sigmac/dmeson.ntu (produced by M.Mattson in 1999). It is a rather clean sample and consists of 6K events. This event sample has overall cuts of $L/\sigma > 6$ and $p_{T\chi} < 14$.

The information about charged particles is taken from standard common blocks of the *recon*-package. We took the D_s candidates reconstructed in *recon* modes of 300 and 301

```
!
! D_s+
!
300 ds+_kkpi      v2 3 +1  k-k+i+      4.  800. 1.569 2.369 $000101
301 ds_-kkpi      v2 3 -1  k-k+i-      4.  800. 1.569 2.369 $000101
```

which corresponds to processes $D_s^\pm \rightarrow K^- K^+ \pi^\pm$,

Reconstruction of partial states is included too:

```
!
! Partial states
!
5 ii0          c 2 0 i+i-      -10. 10. 0.    1.000 $000000
48 pi01        pi0 0 0 g2g2c     0.   0. 0.105 0.165 $000000
49 eta_3pi    ph 2 0 pi0ii0     0.   0. 0.527 0.567 $000000
50 et01        pi0 0 0 g1g1c     0.   0. 0.450 0.650 $000000
```

The D_s candidate mass distribution is shown in Fig. 1. Signal and sideband regions are shaded. The cuts used for all states with D_s below are $L/\sigma > 8$ and $p_{tx} < 8$. Peaks in invariant mass distributions presented below are fitted using P.Cooper's program *gauss.for*. Fit to the D_s peak gives a signal yield of 684.3 ± 33.3 events.

The same distributions for states 300 (D_s^+) and 301 (D_s^-) are shown in Fig. 2 and Fig. 3. The D_s^+ signal yield is 216.9 ± 20.2 events and for D_s^- 467.4 ± 26.2 events.

III. γ -QUANTA RECONSTRUCTION

Detection of gamma-quanta and details of the reconstruction procedure are described in Photon detector note H-828. Neutral-particle-induced clusters in the Photon detectors with visible energy above 0.5 GeV and not associated with any charged track are accepted. A further incident gamma-quanta chi-square cut is made. The reconstruction procedure of π^0 and η meson is described in the Photon paper. Some details are given below. In further analysis invariant mass distributions of mass difference ($D_s^* - D_s$) are used in order to suppress uncertainties in charged particle momentum measurements, where D_s^* refers to any excited (cs) state with a decay mode that we study.

IV. OBSERVATION OF $D_s\gamma$ STATES

The present program is used to reconstruct the $D^{0*}(2007)$ state decaying to $D^0\gamma$ and $D^{0*}\pi^0$. Results are given in the Photon detector note H-828 and are in good agreement with PDG values. Here decay of the $D_s^*(2112)$ state to $D_s\gamma$ ($BR = 95\%$) is studied.

D_s candidates from mass window $1.9685 \pm 0.025\text{GeV}$ and with cuts $L/\sigma > 8$ and $p_{tx} < 8$ (see above) are combined with reconstructed γ -s with energy $E_\gamma > 7\text{GeV}$. The mass difference $M(K^+K^-\pi\gamma) - M(K^+K^-\pi)$ in the region $0.5 - 1\text{ GeV}/c^2$ presented on Fig. 4. A clear $D_s^*(2112)$ signal is observed. The signal is fitted with a gaussian plus a polynomial function for the background as above (the program *gauss.for*). The mass difference of $147.5 \pm 1.8\text{ MeV}/c^2$ is close to the PDG value of $143.9 \pm 0.4\text{ MeV}/c^2$. The signal yield is 105.5 ± 19.57 events. To see influence of experimental conditions in the Photon I detector relative to the Photons II and III we plot the same distribution excluding photons from Photon I (Fig. 5). The new obtained value of mass difference is $147.5 \pm 1.8\text{ MeV}/c^2$ and

is the same as for all detectors. Likewise the signal yield (103.2 ± 22.2 events) and width practically do not change. In the same time number of entries in the histogram (overall background) has dropped by about 30%

This effect, reproduced in simulations, is clearly geometric. The $D_s\gamma$ opening angle is small for $D_{s(2112)}$ decays, and the photon rarely has a wide angle if the D_s^\pm is reconstructed. That is why practically all photons from the $D_{s(2112)}$ signal are detected in the Photon II and III detectors.

Recently a $D_s(2460)$ state decaying to $D_s\gamma$ is observed by Belle and CLEO. We made a search for this state in our data. With the same cuts ($E_\gamma > 7\text{GeV}$, no Photon 1) as in Fig. 5 and at a mass difference region of $0.35 - 0.7\text{GeV}/c^2$ (Fig. 6) we observed a small (about 3σ) peak at $514.8 \pm 4.3\text{ MeV}/c^2$. There is no peak with $M(K^+K^-\pi)$ lying in D_s side bands (see Fig. 1) as shown in Fig. 7. The "mixed event" technique is used to estimate the background. D_s candidates from the current event are combined with γ -s from the previous event to form combinatoric background. The mass difference plot for such combinations $M(K^+K^-\pi\gamma)_{prev} - M(K^+K^-\pi)$ is presented on Fig. 8. No peaks in this region are observed as well. The 3σ peak in the Fig. 6 can be compared with known value of $491\text{MeV}/c^2$ measured by Belle and CLEO. If the peak is real there is a systematics shift of about $20\text{MeV}/c^2$. Such possible big shift in mass is possible due to big value of the photon energy in the decay system and corresponding big angles of photons in the laboratory system. This γ 's are measured in the regions of the detector which have not been precisely calibrated and corrected for non-linearities.

V. $D_s^*(2640) \rightarrow D_s(\eta \rightarrow \gamma\gamma)$

Our search is concentrated on the state decaying to $D_s^* \rightarrow D_s + \eta$. Such state possibly belongs to the same family as recently observed $D_s(2317)$ and $D_s(2460)$ particles in that it decays to a $D_s + pseudoscalar$ with narrow width. We select events with D_s candidate and at least two γ -s each of which has energy $E_\gamma > 2\text{GeV}$ and sum of energies of any pair of γ 's $E_{\gamma\gamma} > 15\text{GeV}$. The upper part of Fig. 9 shows the mass distribution for this selection two-photon combinations. As possible η meson candidates we consider the pairs with invariant mass around a nominal η mass of $547.3\text{ MeV}/c^2$ in the window of $\pm 60\text{ MeV}/c^2$. To suppress combinatorics from multi photon events we select only events

with the number of η candidates less than 5. This distribution is shown in the lower part of Fig. 9 (η and sidebands regions are shaded). A peak of η -meson at mass of $543 \text{ MeV}/c^2$ is seen. Then we kinematically constrained the pairs of γ s in the η region to the nominal η mass value. For $D_s\eta$ combinations passing the above selection criteria we plot mass the difference $\Delta M = M(KK\pi\eta) - M(KK\pi)$ in Fig. 10. A narrow peak at $668.2 \pm 3.4 \text{ Mev}/c^2$ (a $D_s\eta$ mass value of $2637 \text{ Mev}/c^2$) is clearly seen.

A background study is made as following. There are no peaks in this region in distributions of:

- (1) $K^+K^-\pi$ pairs with $M(K^+K^-\pi)$ lying in D_s side bands and combined with a η (Fig. 11);
- (2) D_s candidates combined with $\gamma\gamma$ pairs from the η sidebands (Fig. 12);
- (3)"mixed event" are D_s candidates from current event are combined with γ -s from the previous event (Fig. 13). The fit of background distribution is made by the threshold Fermi function of following form:

$$f = p_1 + (p_2 + p_3 * M_{\gamma\gamma}) / (1 + e^{(M_{\gamma\gamma} - M_\eta)/p_4}) \quad (1)$$

where p_1 to p_4 are parameters of the fit. Then these parameters are used to fit background for the distribution in Fig. 10 using only one normalization parameter. Direct fitting of the effect distribution with this function added with gives better χ^2 and the signal value does not change significantly. It is known that production of D_s mesons is significantly enhanced in the Σ^- beam. We found that majority of $D_s(2640)$ events are produced in this beam as shown in Fig. 14. At the same time background is significantly lower in this case.

Another check of the signal is to plot invariant mass of two unconstrained γ -s in "peak" region $649.86 - 699.05 \text{ MeV}/c^2$. $\Delta M = M(KK\pi\eta) - M(KK\pi)$ distribution for several cuts presented on Fig. 15. As we plot the 2γ invariant mass for γ 's passing the cuts above, the η meson signal is clearly seen. There is a significant enhancement in the η signal for events from the $D_s(2640)$ peak region.

VI. $D_s^*(2640) \rightarrow D_s(\eta \rightarrow \pi^-\pi^+\pi^0)$

Confirmation of the observed signal should come from a study of the process $D_s^* \rightarrow D_s\eta$ where $\eta \rightarrow \pi^-\pi^+\pi^0$. To reconstruct decay $\eta \rightarrow \pi^-\pi^+\pi^0$ we took pairs of $\pi^-\pi^+$ (*Recon5*) in

which the π^- and π^+ are not used in $K^+K^-\pi$ system forming D_s candidate. We required the sum of pion momenta $p(\pi^+) + p(\pi^-) > 8GeV/c$. Next we added γ pairs in the π^0 mass window of $135 \pm 7.5 MeV/c^2$ which has both γ energies $E_\gamma > 2GeV$ (no kinematic fit of $\gamma\gamma$ pair mass to the π^0 mass).

We accept as η decay candidates $\pi^-\pi^+\pi^0$ events with an invariant mass in the window $547.3 \pm 60 MeV/c^2$ (the same cut as for $\gamma\gamma$ mode). Only events with number of these η candidates less than 5 are accepted. The resulting distribution for the 3 pion system is presented in Fig 16. Note again that there are no constraints to the π^0 nominal mass or to the η nominal mass. For $D_s\eta$ combinations satisfying all requirements above we plot mass difference $\Delta M = M(KK\pi\eta) - M(KK\pi)$ presented on Fig. 17. A narrow peak at 678.4 ± 5.9 corresponds to mass $2647 MeV/c^2$ clearly seen. As before for the channel $D_s^*(2640) \rightarrow D_s(\eta \rightarrow \gamma\gamma)$ we studied following background distributions:

1. $K^+K^-\pi$ pairs with $M(K^+K^-\pi)$ in D_s side bands are combined with a η , see Fig. 18 (D_s sideband);
2. D_s candidates are combined with $\pi^-\pi^+\pi^0$ combinations from η sidebands, see Fig. 19 (η sideband);
3. D_s candidates from current event have been combined with $\pi^-\pi^+\pi^0$ combination from the previous event, see Fig. 20, ("mixed event").

There are no peaks in the region of interest observed in all these distributions. Invariant mass $M(\pi^-\pi^+\pi^0)$ distribution in the $D_s^*(2640) \rightarrow D_s(\eta \rightarrow \pi^-\pi^+\pi^0)$ "peak" region $0.64986 - 0.69905$ is investigated in the same way as for $\eta \rightarrow \gamma\gamma$. The $\Delta M = M(KK\pi\eta) - M(KK\pi)$ distribution for several cuts presented in Fig. 21. Enhancement in η mass region for events in the peak region is seen.

VII. SIGNAL SYSTEMATICS STUDIES.

There are several studies of signal systematics:

1. background subtraction ;
2. re-binning and signal variations;
3. variations of γ -quanta energy corrections procedures with constrains on π^0 and η masses.

The various types of the background shapes described above are used to evaluate sys-

tematics. The "mixed event" and "side band" backgrounds are normalized on the area of the main distribution above the peak and then substracted from it. All of them give similar results with variations of number of peak events ± 5 .

Re-binning the main histogramm with bins shifted by $5 \text{ MeV}/c^2$ is shown on Fig. 22-23. There is increase of number of fitted events but this change remains within the statisctical error.

The study of the γ -quanta energy measurements is made for the most difficult $\eta \rightarrow \pi^- \pi^+ \pi^0$ decay mode. Above we made no constrain on the masses of π^0 and η mesons. The peak of η is shifted by about $15 \text{ MeV}/c^2$. This results in shift of the $D_s(2640)$ peak position by $10\text{-}12 \text{ MeV}/c^2$.

As we plot the mass difference $\Delta M = M(KK\pi\eta) - M(KK\pi)$ ($\eta \rightarrow \pi^- \pi^+ \pi^0$) for events without Photon1 detector, (Fig. 24) position of the peak is shifted to $671 \text{ MeV}/c^2$ which is only 4 MeV from value in the decay mode $D_s^*(2640) \rightarrow D_s(\eta \rightarrow \gamma\gamma)$. Possibly the peak shift observed above for the 3π mode is due to insufficient calibration and/or nonlinearities of the Photon 1. Further, a constrain on the π^0 and η masses is applied and position of the peak in 3π mode agreed with one for 2γ mode within $3 \text{ MeV}/c^2$ for all Photon detectors.

VIII. SOME PROPERTIES OF THE SIGNAL.

Next thing would be separating distributions for $D_s^+\eta$ and $D_s^-\eta$ invariant mass. Fig. 25 and Fig. 26 show distributions for D_s^+ mode, id=300 for $\eta \rightarrow \gamma\gamma$ and $\eta \rightarrow \pi^- \pi^+ \pi^0$ decays. The signal is seen in both η decay modes but fitted peak width is somewhat wider than for full sample.

Fig. 27 and Fig. 28 show distributions for D_s^- mode, id=301 for $\eta \rightarrow \gamma\gamma$ and $\eta \rightarrow \pi^- \pi^+ \pi^0$ decays. The signal is seen in $\eta \rightarrow \gamma\gamma$ decay mode and none is seen in three pions decay mode.

Further distributions for events in signal and sidebands regions (as shown in Fig. 29, where selected regions are shaded) are compared. Momentum distributions along the beam P_z for D_s^η are shown for these two regions in Fig. 30 and Fig. 31 correspondingly.

Relative momentum $p_z(D_s)/p_z(D_s\eta)$ distributions for signal and side band regions presented in Fig. 32 and Fig. 33 correspondingly. There are no significant differences between the peak and side band regions for all above distributions.

η helicity angle $\cos(\theta^*(\eta))$ distributions for process $D_s^*(2640) \rightarrow D_s(\eta \rightarrow \gamma\gamma)$ and $D_s^*(2640) \rightarrow D_s(\eta \rightarrow \pi^-\pi^+\pi^0)$ in the peak region are presented in Fig. 34 and Fig. 35 correspondingly. The same distributions but in sideband region presented at Fig. 36.

The distributions are looks similar but side band events are more peaked to backward direction of flight of η in the decay center of mass system. Limited statistics and relatively big level of background do not allow to make any conclusions about spin of the observed state.

IX. MONTE CARLO SIGNAL SIMULATIONS

The program *EmbeddedDataGenerator for SELEX* or *EDG* based on the event generator *QQ* from CLEO (see also SELEX web page) is used to generate files for various decay modes of the new state $D_s^*(2640) \rightarrow D_s\eta$ as well as for several other known charm states.

D_s^* events are generated with zero decay width separately for two η decay modes: $\eta \rightarrow \gamma\gamma$ and $\eta \rightarrow \pi^-\pi^+\pi^0$ with subsequent decay $\pi^0 \rightarrow \gamma\gamma$. Files are generated for D_s^+ and D_s^- mesons. Only decay $D_s \rightarrow KK\pi$ is considered. To verify the calculations events with decays of $D_s(2112) \rightarrow D_s\gamma$ are generated with standard parameters (only $D_s \rightarrow KK\pi$ is considered).

For testing the detector response and to determine process efficiency the tracks generated by the EDG program are imported into GEANT program SELEX GE781. This package is used by V. Molchanov and I. Larin to analyze *A2* and *B2* mesons. In this study we pay special attention to the Photon detector parameters in order to understand them better. The output of the GE781 generator contains events in a standard event format of SELEX experiment. These generated events are processed with the same reconstruction package as the real ones. The efficiencies for D_s including secondary vertex reconstruction and $D_s^*(2640) \rightarrow D_s\eta$ in two η decay modes are found. The results are shown on Table 1 and in Fig. 37-46 for reconstruction of η decays to $\gamma\gamma$ and $\pi^-\pi^+\pi^0$ in events with D_s^- and then $D_s^-\eta$ states. In addition the results of simulations of signal of $D_s^*(2112)$ in distribution of $M(K^+K^-\pi\gamma) - M(K^+K^-\pi)$ presented on Fig. 47 and 48.

First, we found that the experimental resolution of the Photons for η decays in events with D_s is well decribed by Monte Carlo simulations as shown in Fig. 37-38. Only distributions for events containing $K^+K^-\pi^-$ system are plotted, since $K^+K^-\pi^+$ ones are similar.

These distributions presented for two decays modes $\eta \rightarrow \gamma\gamma$ and $\eta \rightarrow \pi^-\pi^+\pi^0$ are calculated under the same cuts as experimental ones Fig. 15 and 21. Monte Carlo generated mass distributions for $K^+K^-\pi^-$ and $K^+K^-\pi^+$ (D_s^- and D_s^+ signals) and $K^+K^-\pi^-\eta$ and $K^+K^-\pi^+\eta$ are presented in Fig. 39-46.

All distributions are presented for two η decay modes considered. Note that efficiencies for reconstruction of D_s in events with $\eta \rightarrow \gamma\gamma$ and $\eta \rightarrow \pi^-\pi^+\pi^0$ can be somewhat different. To check it mass distributions for each η decay mode presented: $K^+K^-\pi$, $K^+K^-\pi\eta$ and two charges of π in the $K^+K^-\pi$ system. Differences between these Monte Carlo distributions are found to be small compared with experimental uncertainties. The simulated width of the newly found $D_s\eta$ state is close to experimental value of 12 -15 Mev.

Second, we calculated relative efficiencies for the decay modes of: $D_s^*(2640) \rightarrow D_s(\eta \rightarrow \gamma\gamma)$ and $D_s^*(2640) \rightarrow D_s(\eta \rightarrow \pi^-\pi^+\pi^0)$. The number of observed events corrected for Monte Carlo detection efficiencies and known η branching ratios are presented in Table 1. About 40% of the observed D_s come from the newly observed state. The number of observed events in two decay modes $\eta \rightarrow \gamma\gamma$ and $\eta \rightarrow \pi^-\pi^+\pi^0$ are compatible with known decay branching ratio (within big errors) but corrected number of events from 3π mode is on the high side. Observed width of the decay $D_s(2112) \rightarrow D_s\gamma$ is also compatible with calculated resolution. About 30% of all detected D_s are coming from this source.

X. CONCLUSIONS

We report observation of new narrow $D_s^*(2640)$ meson in the decay mode $D_s^*(2640) \rightarrow D_s\eta$. Peaks of 43 ± 11 events at $D_s(\eta) - D_s$ mass difference distribution at 668 ± 3 MeV/c² in the decay mode $D_s^*(2640) \rightarrow D_s(\eta \rightarrow \gamma\gamma)$ and of 22 ± 7 events with 678 ± 6 MeV/c² in mode $D_s^*(2640) \rightarrow D_s(\eta \rightarrow \pi^-\pi^+\pi^0)$ with statistical significance 5.1σ and 4.6σ correspondently are found. We suggest that this is a new state of the D_s^* family.

1. $D_s\eta$ efficiencies by Monte Carlo and corrected event number

Decay mode	Generated events	Passed events	Detection efficiency	Observed events	Corrected events	Total event fraction
$D_s(\eta \rightarrow \gamma\gamma)$	19489	6930	0.355	43(11)	299(77)	0.44(0.11)
$D_s(\eta \rightarrow 3\pi)$	19257	1519	0.079	21(7)	108(34)	1.1(0.4)
$D_s^*(2112) \rightarrow D_s\gamma$	13730	6448	0.47	105(20)	235(47)	0.34(0.07)

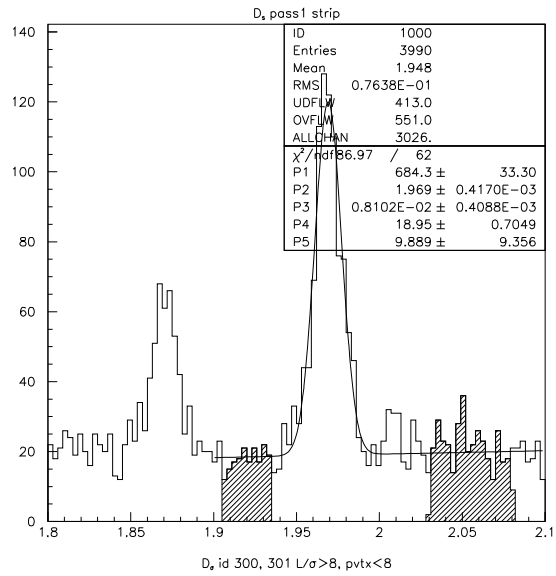


FIG. 1: ($K^+K^-\pi$) with $L/\sigma > 8$ and $pvtx < 8$.

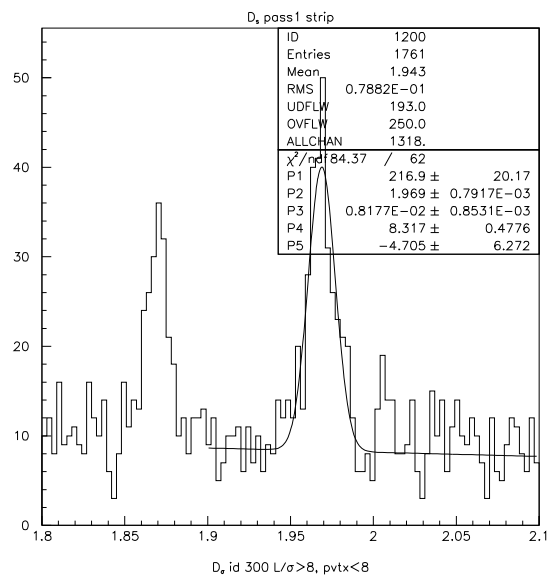


FIG. 2: ($K^+K^+\pi^+$) with $L/\sigma > 8$ and $pvtx < 8$

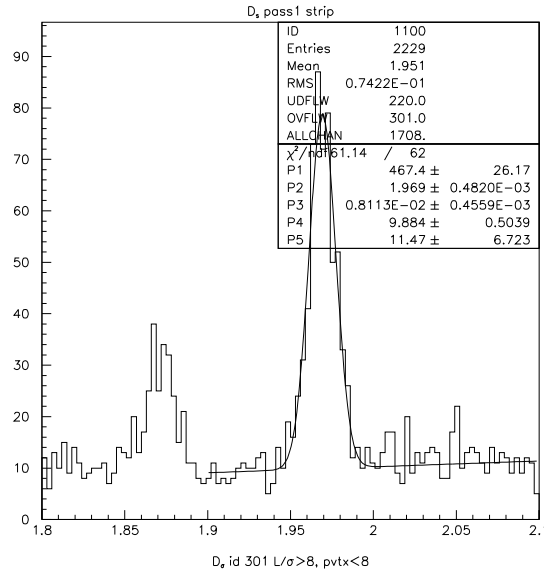


FIG. 3: $(K^+ K^- \pi^-)$ with $L/\sigma > 8$ and $pvtx < 8$

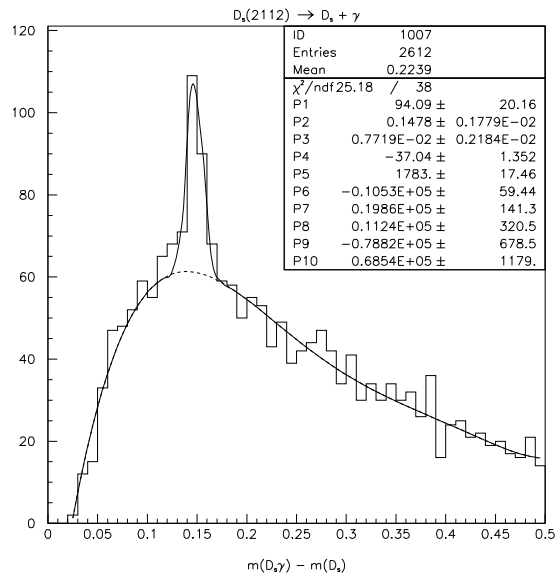


FIG. 4: $M(K^+ K^- \pi\gamma) - M(K^+ K^- \pi)$

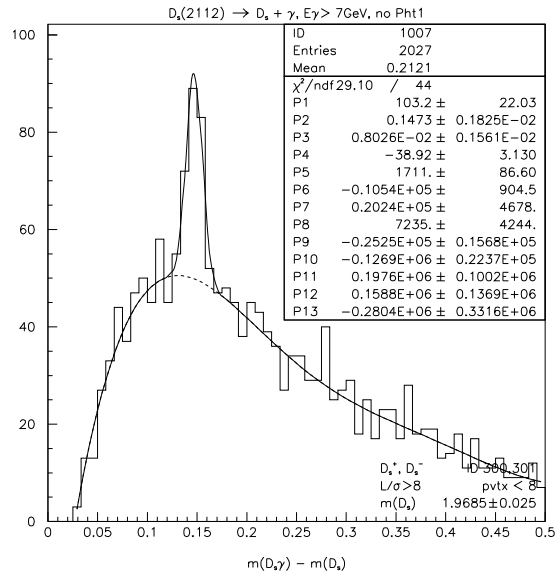


FIG. 5: $M(K^+K^-\pi\gamma) - M(K^+K^-\pi)$

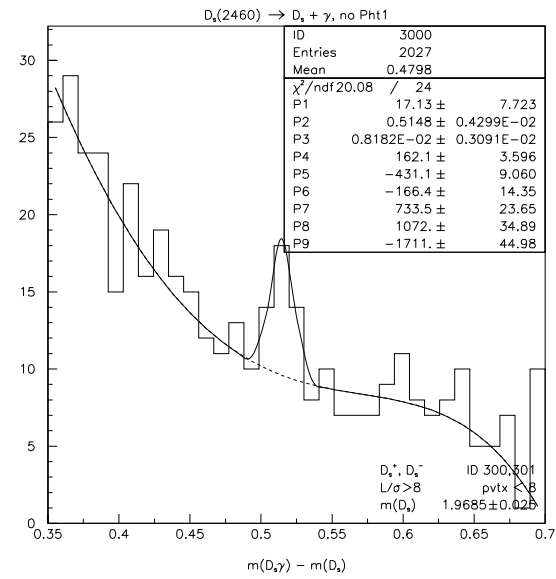


FIG. 6: $M(K^+K^-\pi\gamma) - M(K^+K^-\pi)$

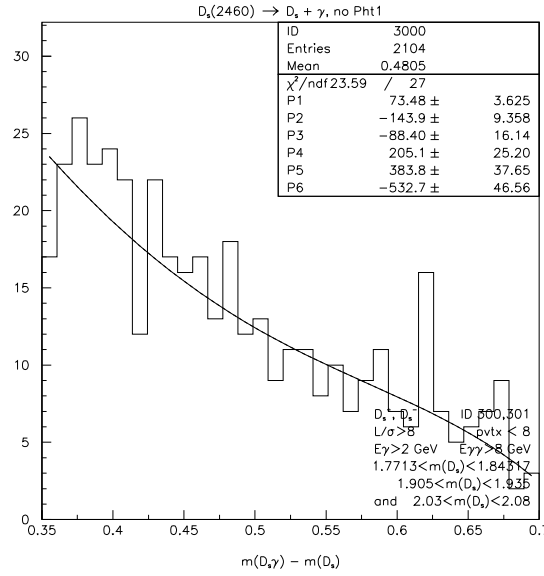


FIG. 7: $M(K^+K^-\pi\gamma) - M(K^+K^-\pi)$ from D_s sideband region

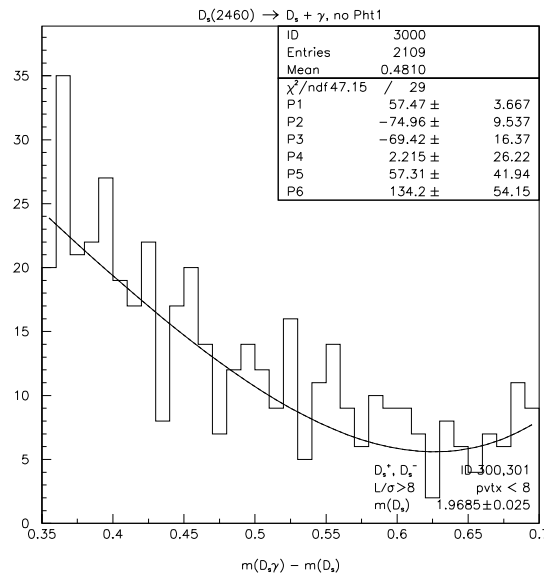


FIG. 8: $M(K^+K^-\pi\gamma) - M(K^+K^-\pi)$ from D_s "mixed events"

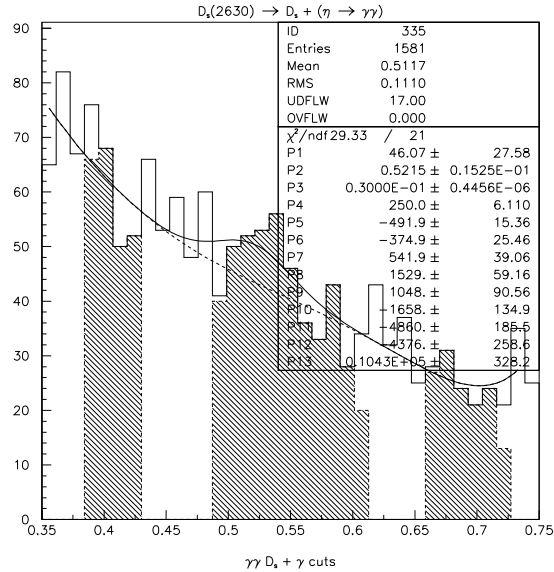


FIG. 9: $M(\gamma\gamma)$ with $E_\gamma > 2GeV$, $E_{\gamma\gamma} > 8GeV$ in η meson mass region.

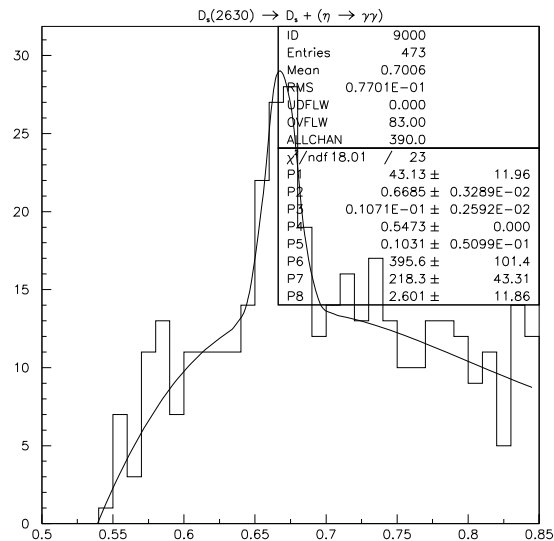


FIG. 10: $M(K^+K^-\pi\eta) - M(K^+K^-\pi)$

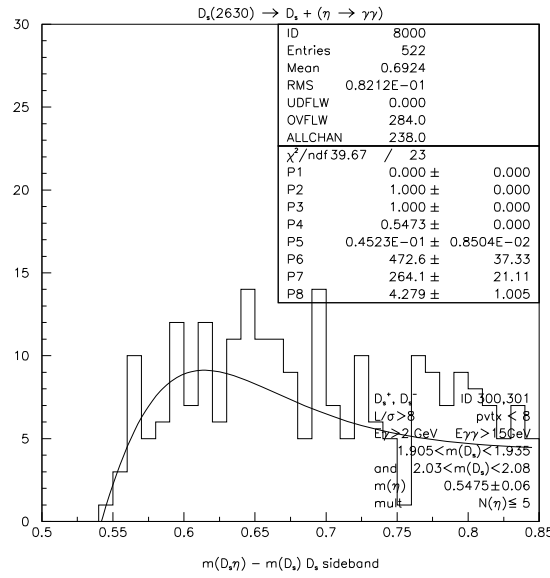


FIG. 11: $M(K^+K^-\pi\eta) - M(K^+K^-\pi)$ from D_s sidebands region

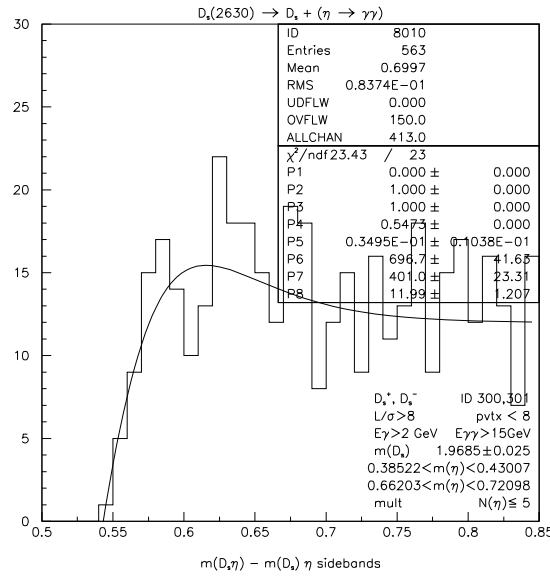


FIG. 12: $M(K^+K^-\pi\eta) - M(K^+K^-\pi)$ from η sidebands region

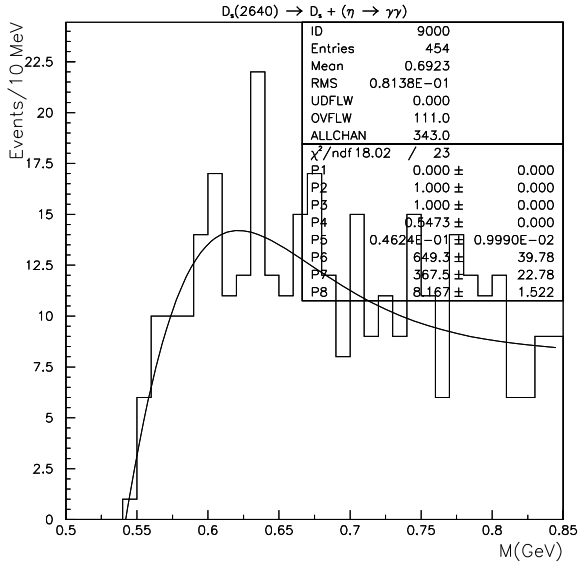


FIG. 13: $M(K^+K^-\pi\eta) - M(K^+K^-\pi)$ from mixed event

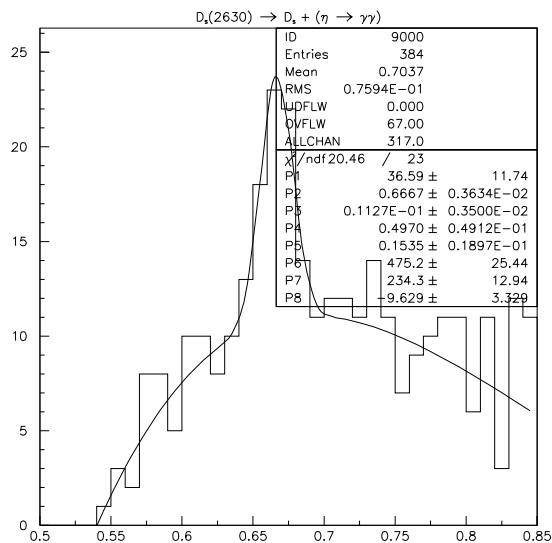


FIG. 14: $M(K^+K^-\pi\eta) - M(K^+K^-\pi)$ for Σ^- beam

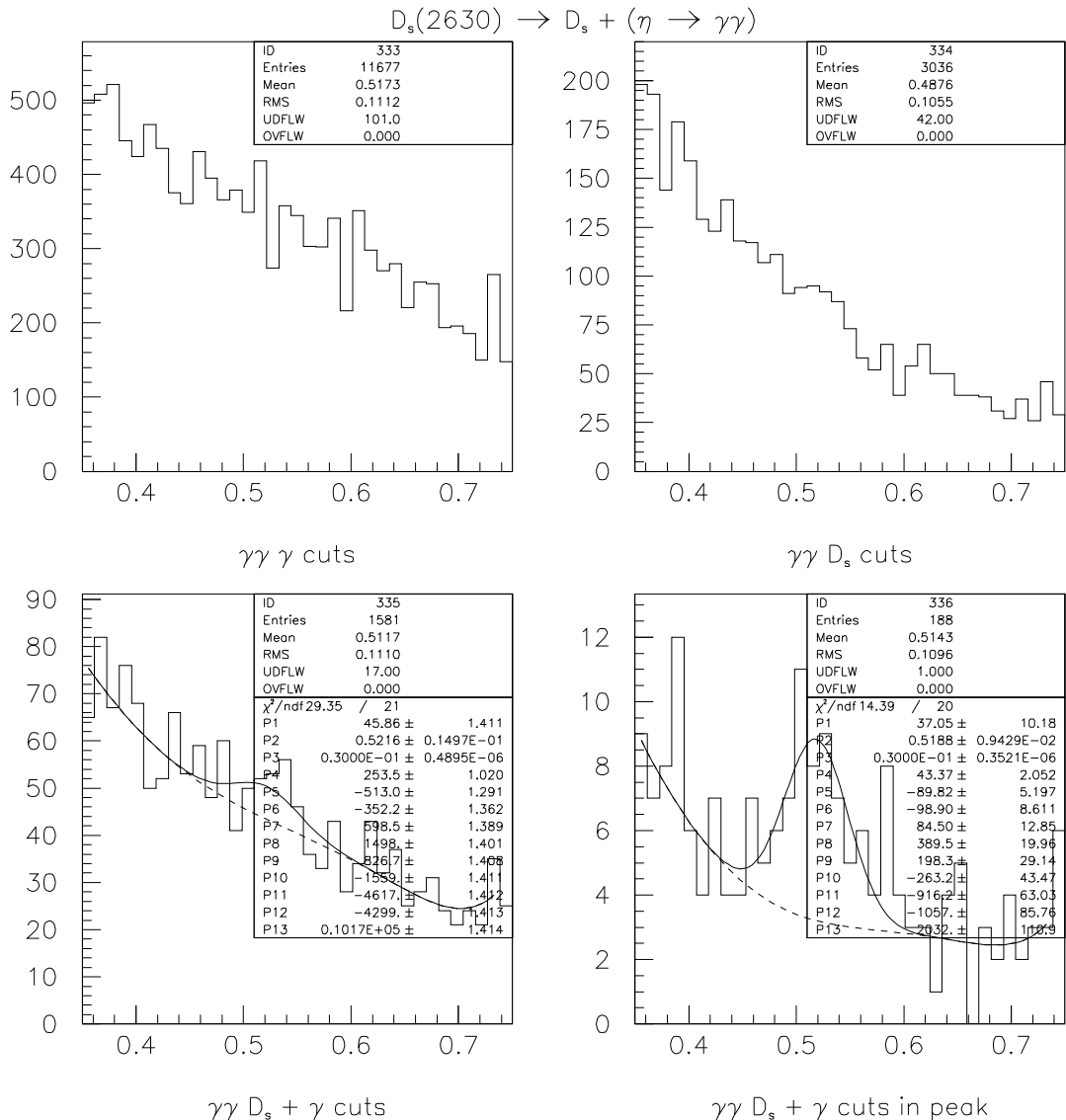


FIG. 15: $M(\gamma\gamma)$ in η region for different cuts

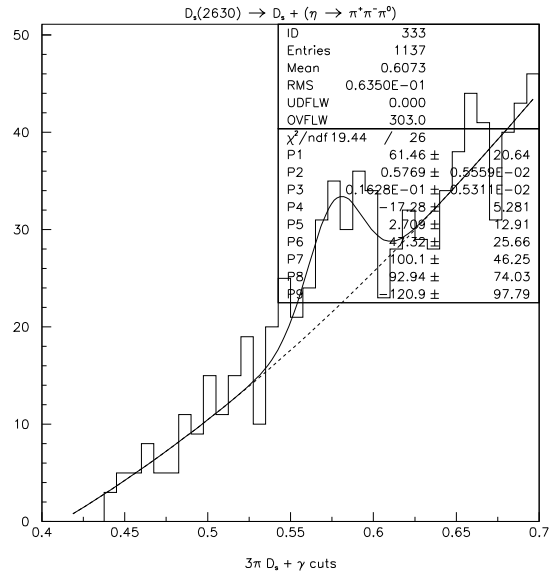


FIG. 16: $M(\pi^-\pi^+\pi^0)$

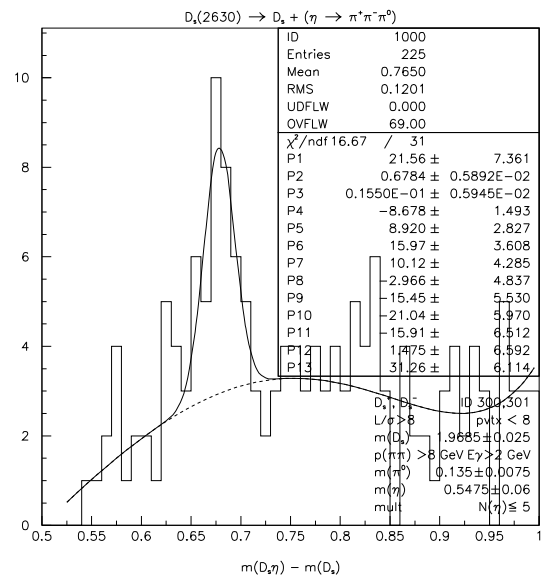


FIG. 17: $M(K^+K^-\pi\eta) - M(K^+K^-\pi)$ for $\eta \rightarrow \pi^-\pi^+\pi^0$

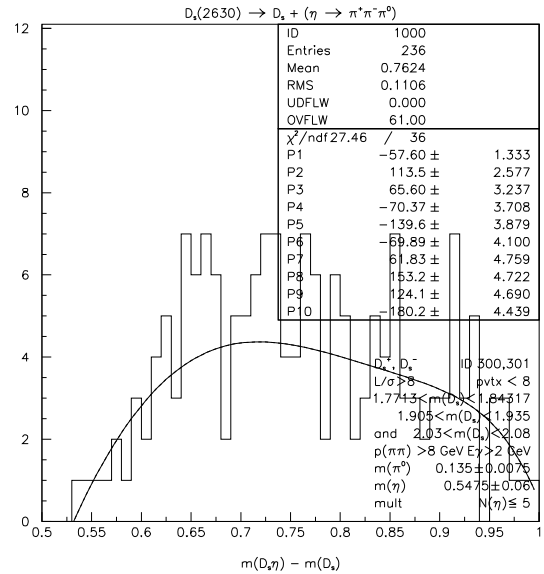


FIG. 18: $M(K^+K^-\pi\eta) - M(K^+K^-\pi)$ from D_s sidebands region

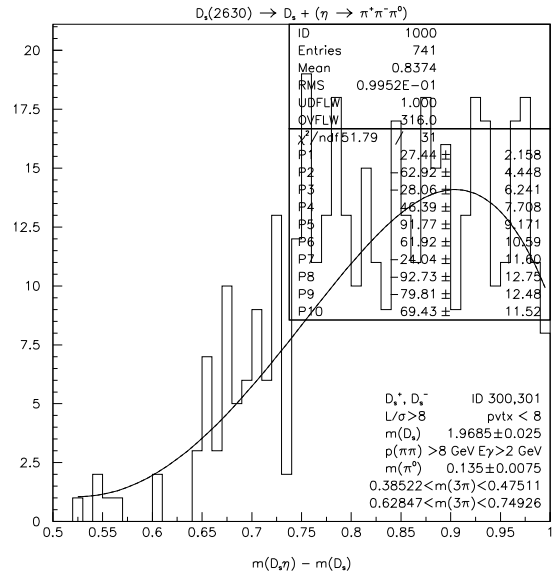


FIG. 19: $M(K^+ K^- \pi\eta) - M(K^+ K^- \pi)$ from η sideband region

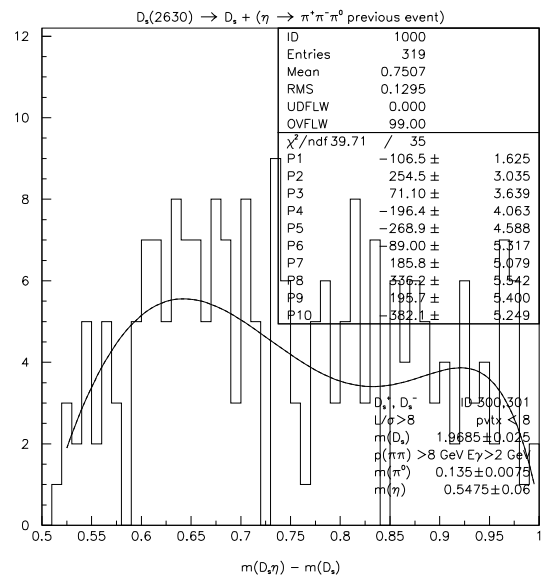


FIG. 20: $M(K^+ K^- \pi\eta) - M(K^+ K^- \pi)$ for mixed event

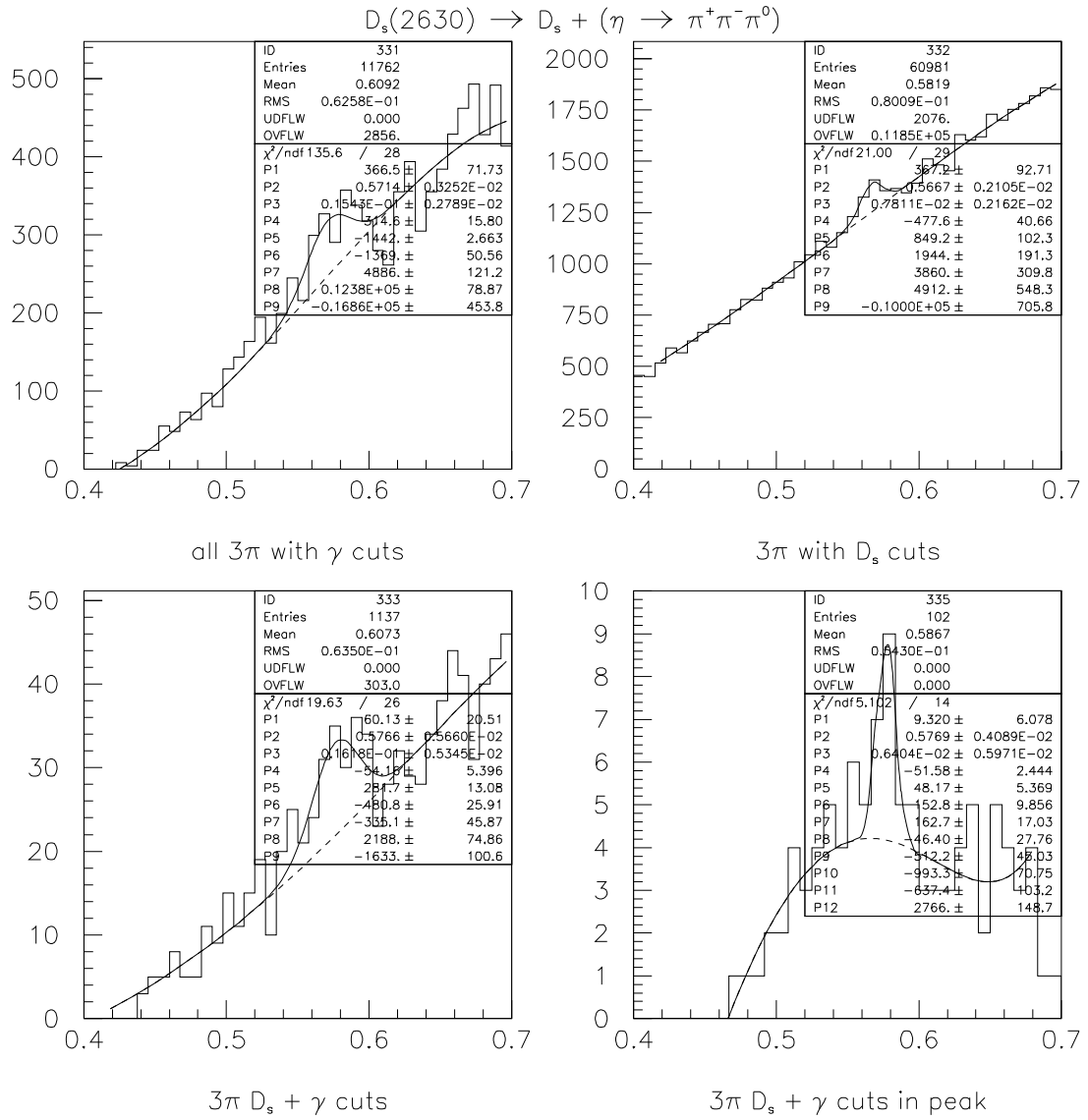


FIG. 21: $M(\pi^- \pi^+ \pi^0)$ in η region for different cuts

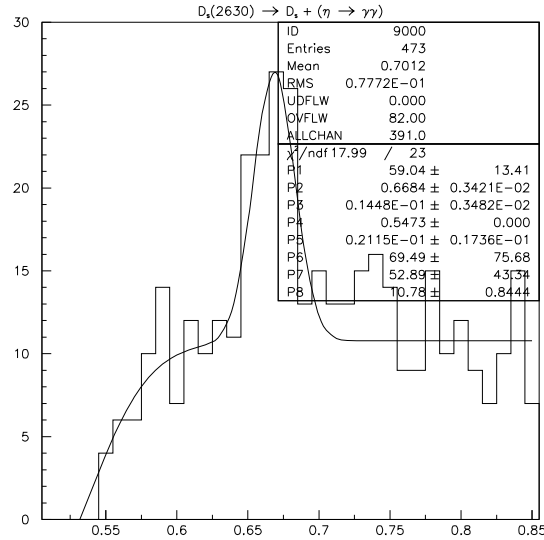


FIG. 22: $M(K^+K^-\pi\gamma) - M(K^+K^-\pi)$ $\eta \rightarrow \gamma\gamma$ bin shift by 0.005

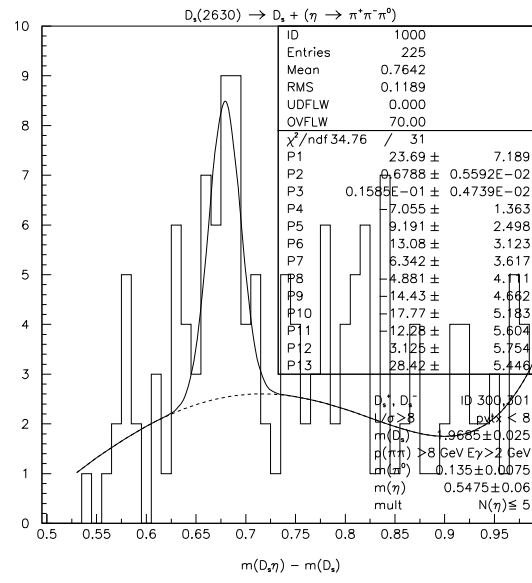


FIG. 23: $M(K^+K^-\pi\gamma) - M(K^+K^-\pi)$ and $\eta \rightarrow \pi^-\pi^+\pi^0$ bin shift by 0.005

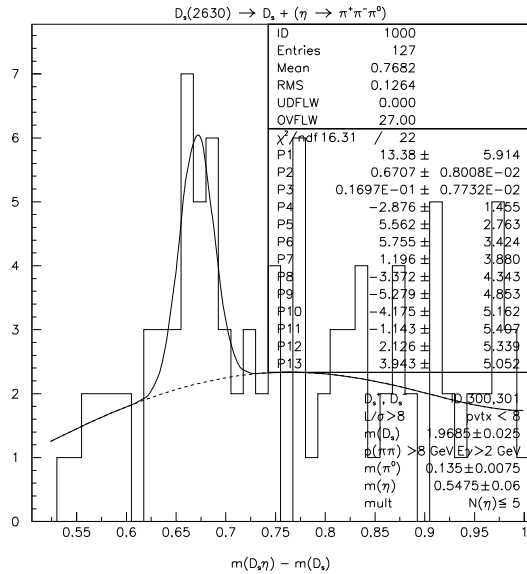


FIG. 24: $M(K^+K^-\pi\eta) - M(K^+K^-\pi)$ for $\eta \rightarrow \pi^-\pi^+\pi^0$ no Photon 1

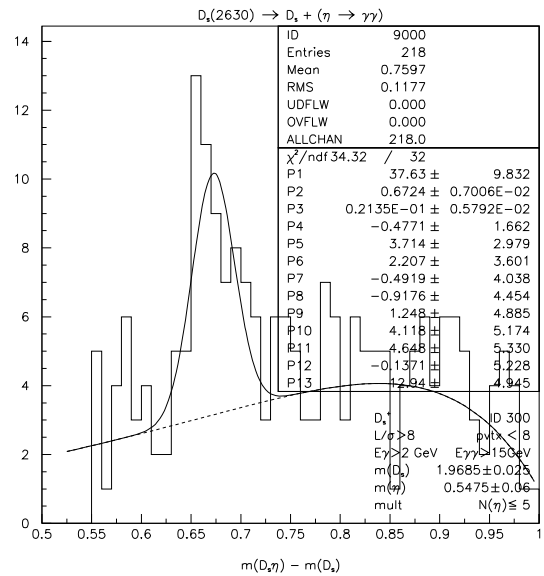


FIG. 25: $M(K^+K^-\pi\eta) - M(K^+K^-\pi)$ for D_s^+ and $\eta \rightarrow \gamma\gamma$

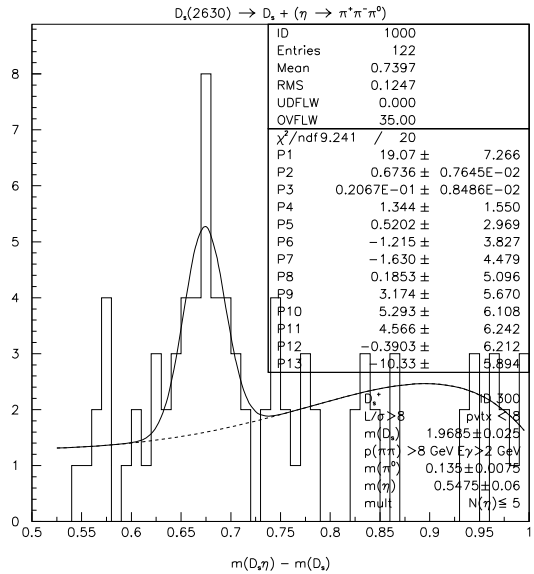


FIG. 26: $M(K^+K^-\pi\eta) - M(K^+K^-\pi)$ for $D_s^+ \eta \rightarrow \pi^-\pi^+\pi^0$

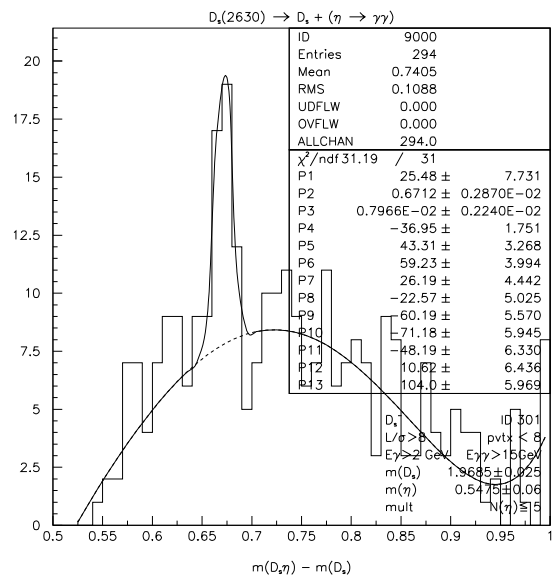


FIG. 27: $M(K^+K^-\pi\eta) - M(K^+K^-\pi)$ for D_s^- and $\eta \rightarrow \gamma\gamma$

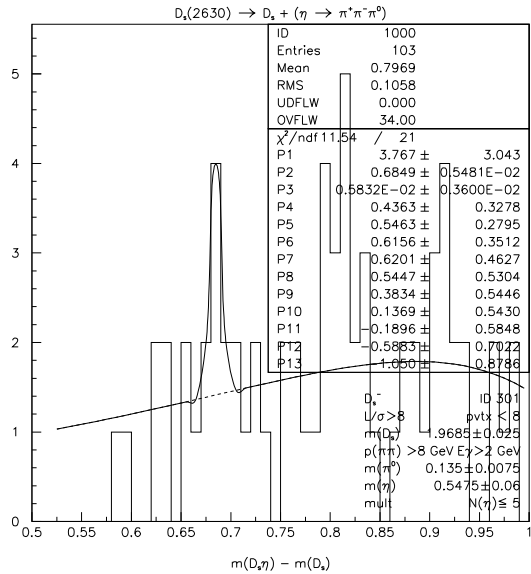


FIG. 28: $M(K^+K^-\pi\eta) - M(K^+K^-\pi)$ for D_s^- and $\eta \rightarrow \pi^-\pi^+\pi^0$

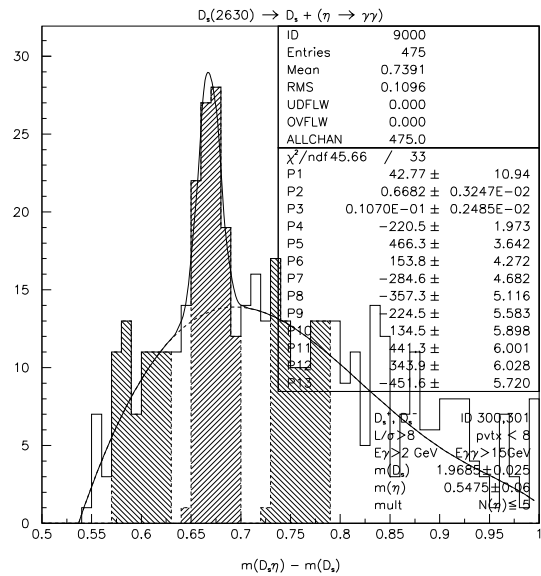


FIG. 29: $M(K^+K^-\pi\eta) - M(K^+K^-\pi)$

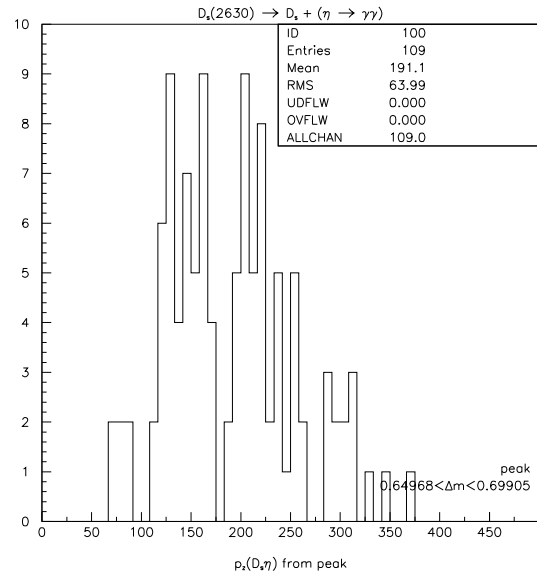


FIG. 30: $p_z(D_s \eta)$ for signal region

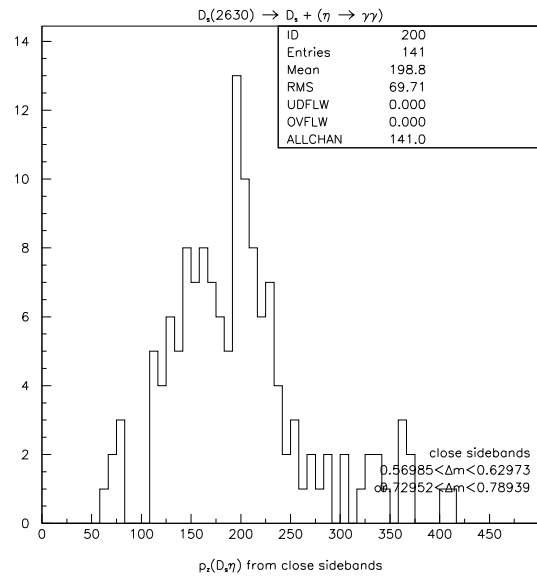


FIG. 31: $p_z(D_s \eta)$ for sideband region

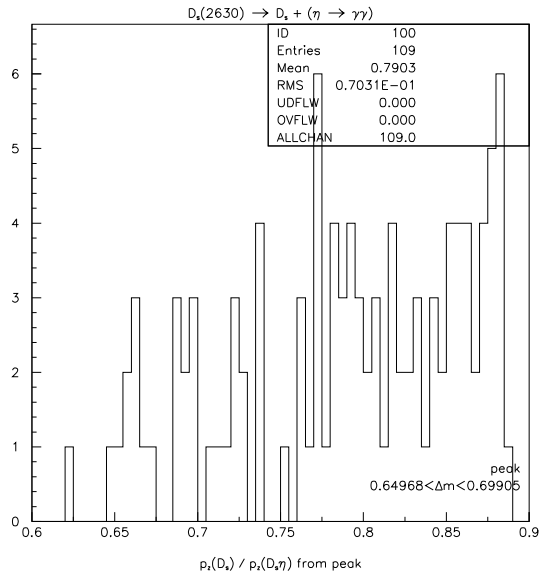


FIG. 32: $p_z(D_s) / p_z(D_s\eta)$ for signal region

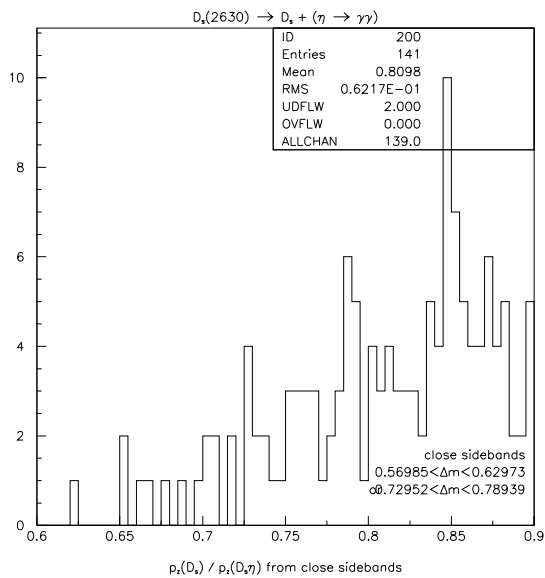


FIG. 33: $p_z(D_s) / p_z(D_s\eta)$ for sideband region

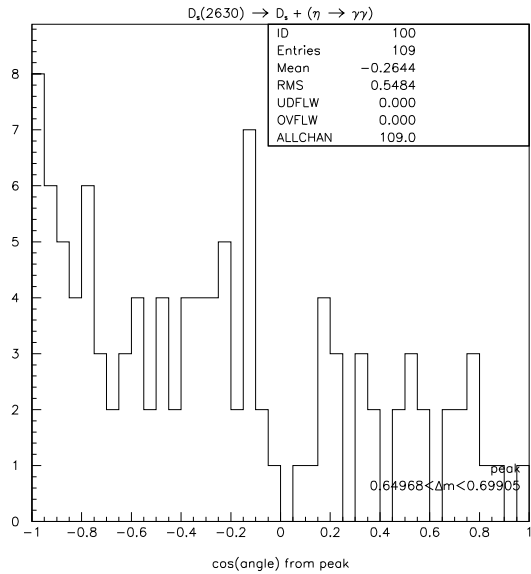


FIG. 34: The $D_s^*(2640) \rightarrow D_s(\eta \rightarrow \gamma\gamma)$ helicity distribution for peak region.

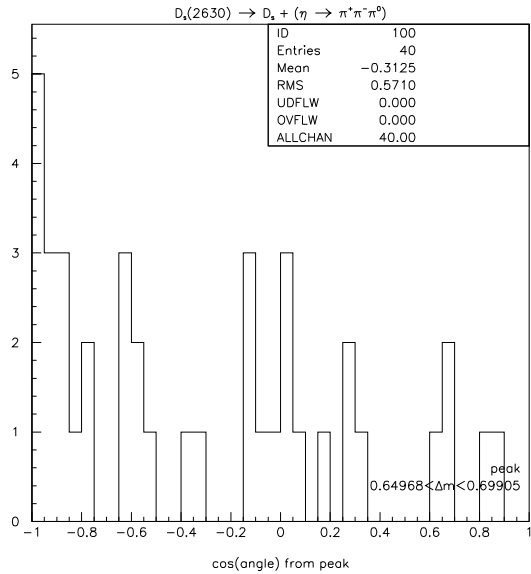


FIG. 35: The helicity distribution for $D_s^*(2640) \rightarrow D_s(\eta \rightarrow \pi^-\pi^+\pi^0)$ peak region.

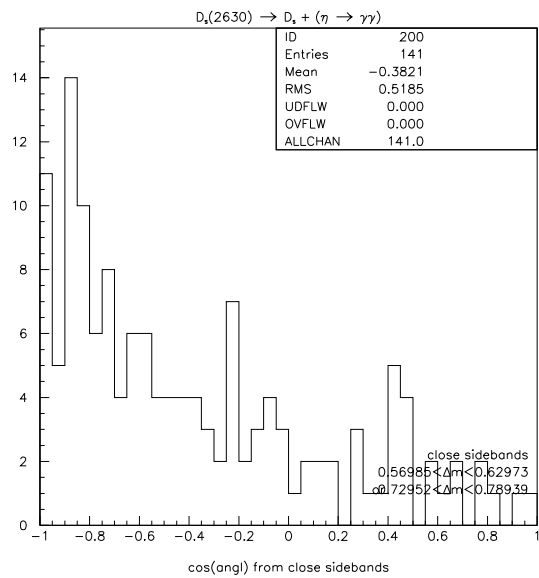


FIG. 36: The $D_s^*(2640) \rightarrow D_s(\eta \rightarrow \gamma\gamma)$ helicity distribution for sideband region.

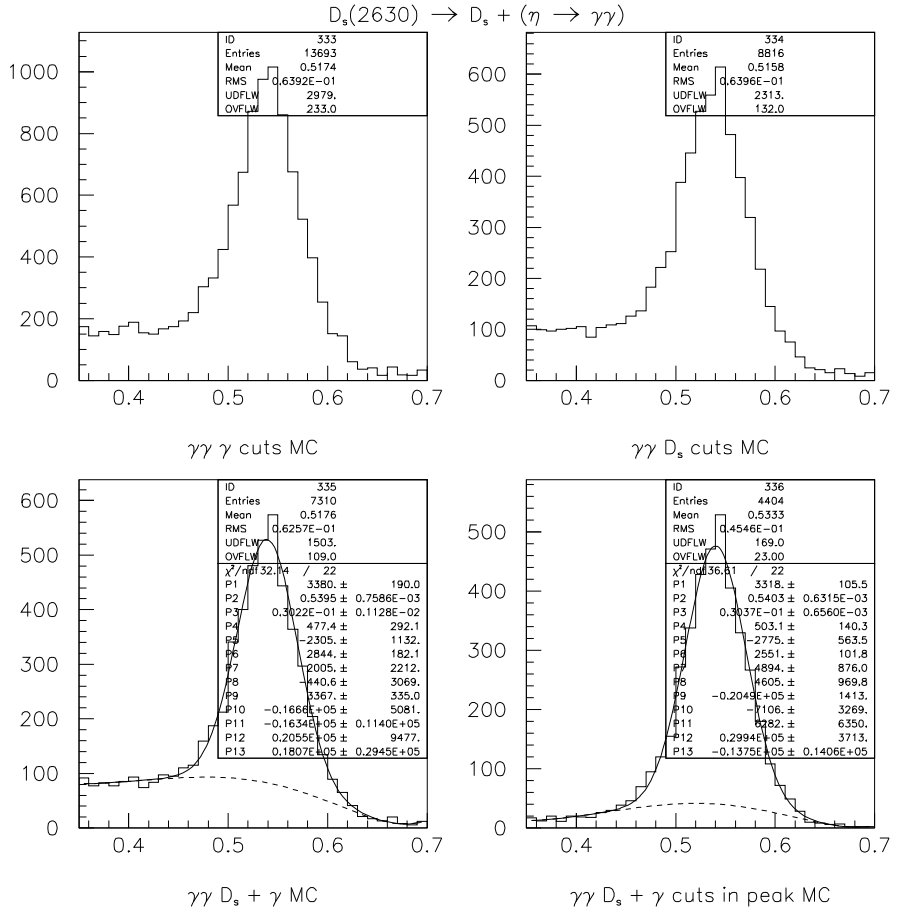


FIG. 37: Monte Carlo: $M(K^+K^-\pi\eta) - M(K^+K^-\pi^-)$ for $\eta \rightarrow \gamma\gamma$

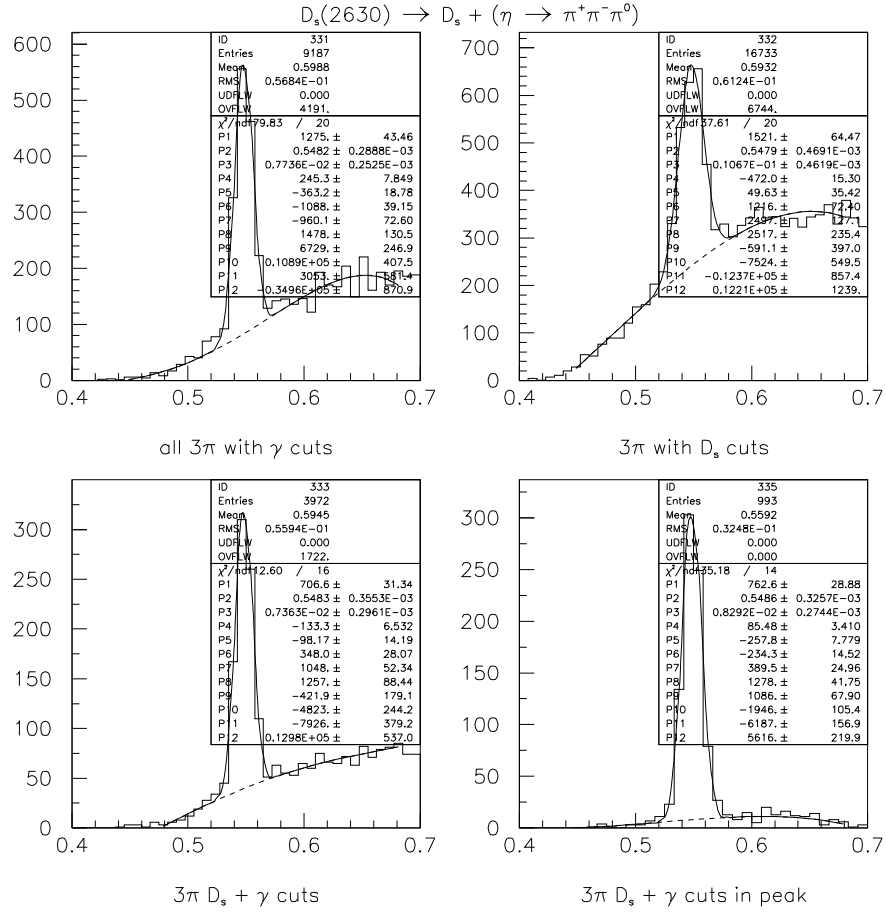


FIG. 38: Monte Carlo: $M(K^+K^-\pi^\eta) - M(K^+K^-\pi)$ for $\eta \rightarrow \gamma\gamma$

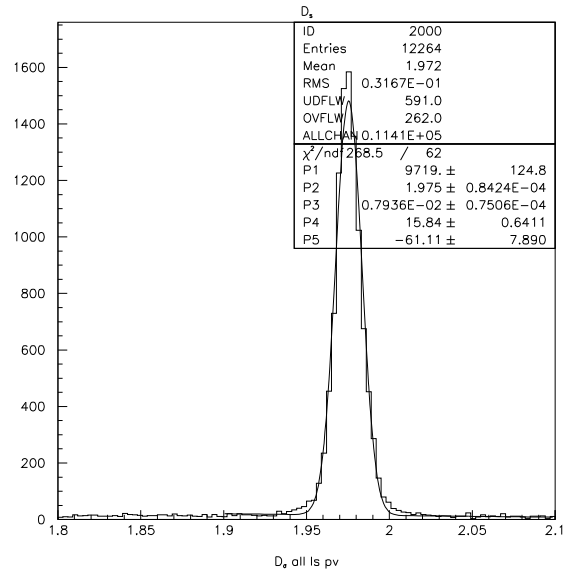


FIG. 39: Monte Carlo: M($K^+K^-\pi^-$) with $L/\sigma > 8$ and $pvtx < 8$.

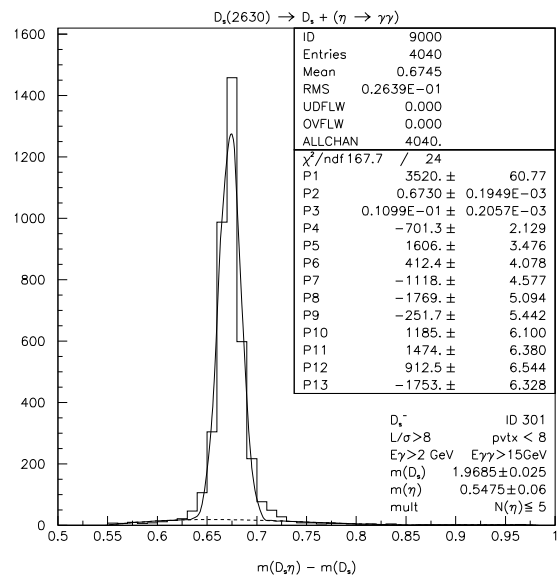


FIG. 40: Monte Carlo: M($K^+K^-\pi^-\eta$) - M($K^+K^-\pi^-$) for $\eta \rightarrow \gamma\gamma$

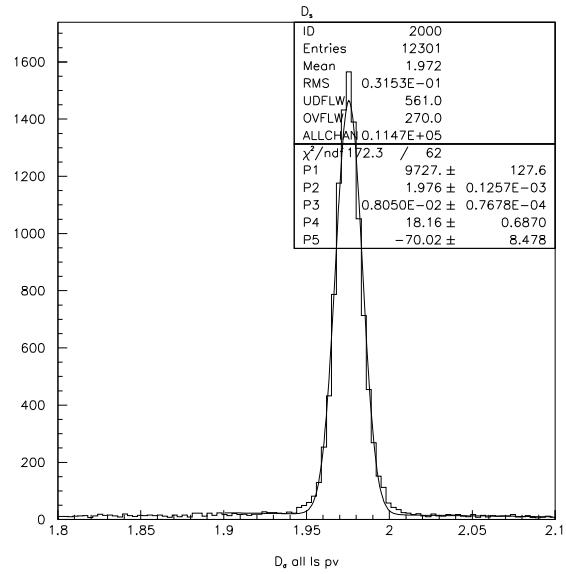


FIG. 41: Monte Carlo: M($K^+K^-\pi^+$) with $L/\sigma > 8$ and $pvt x < 8$.

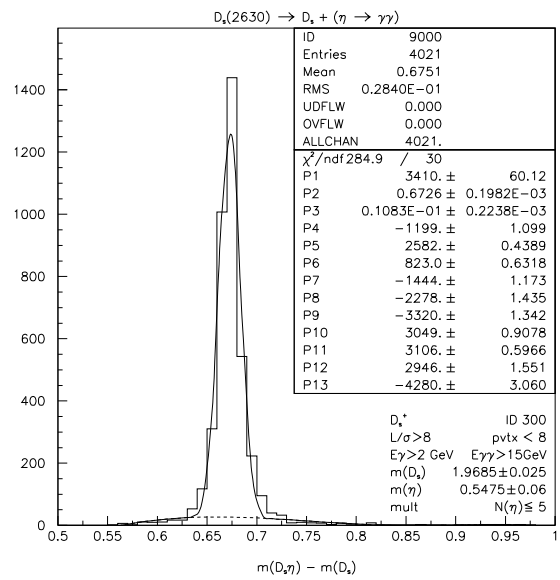


FIG. 42: Monte Carlo: M($K^+K^-\pi^+\eta$) - M($K^+K^-\pi^+$) for $\eta \rightarrow \gamma\gamma$

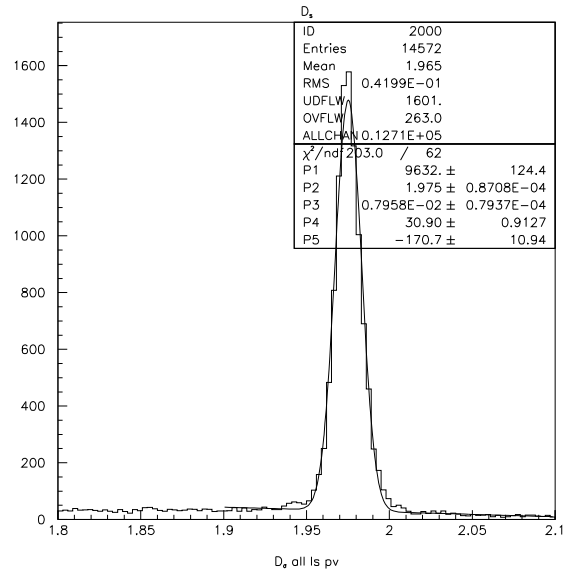


FIG. 43: Monte Carlo: M($K^+K^-\pi^-$) with $L/\sigma > 8$ and $pvt x < 8$.

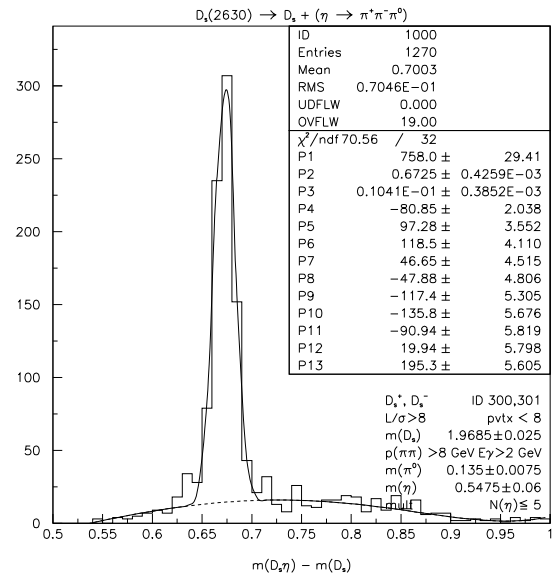


FIG. 44: Monte Carlo: M($K^+K^-\pi^-\eta$) - M($K^+K^-\pi^-$) for $\eta \rightarrow \pi^-\pi^+\pi^0$

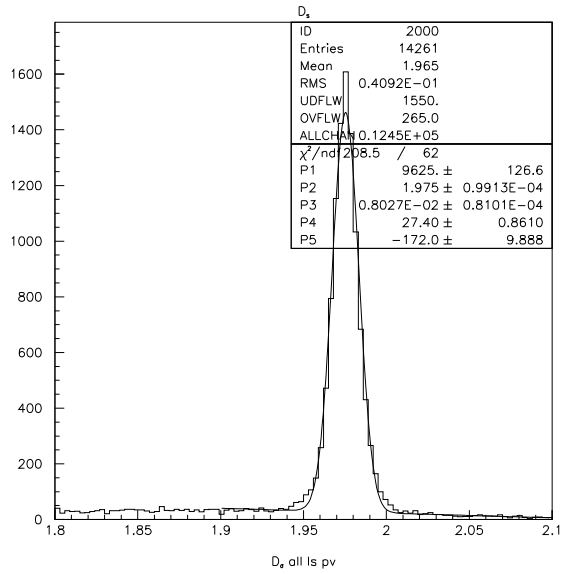


FIG. 45: Monte Carlo: M($K^+K^-\pi^+$) with $L/\sigma > 8$ and $pvtx < 8$.

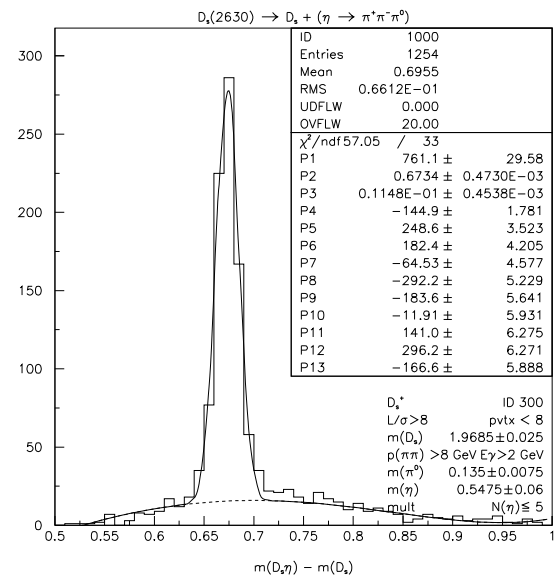


FIG. 46: Monte Carlo: M($K^+K^-\pi^+\eta$) - M($K^+K^-\pi^+$) for $\eta \rightarrow \pi^-\pi^+\pi^0$

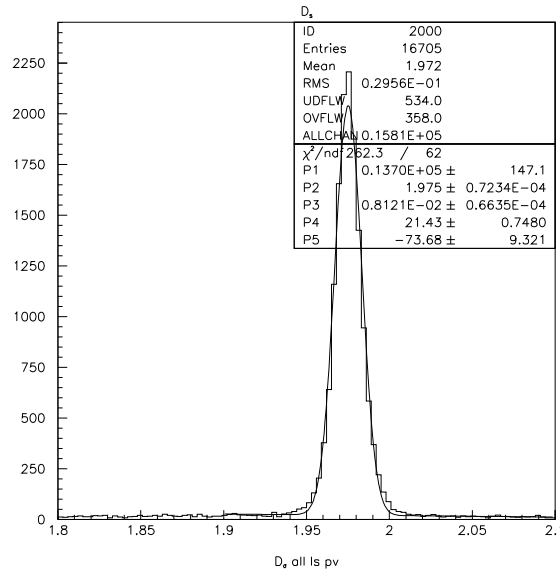


FIG. 47: Monte Carlo: M($K^+K^-\pi$) with $L/\sigma > 8$ and $pvtx < 8$. for D_s^*

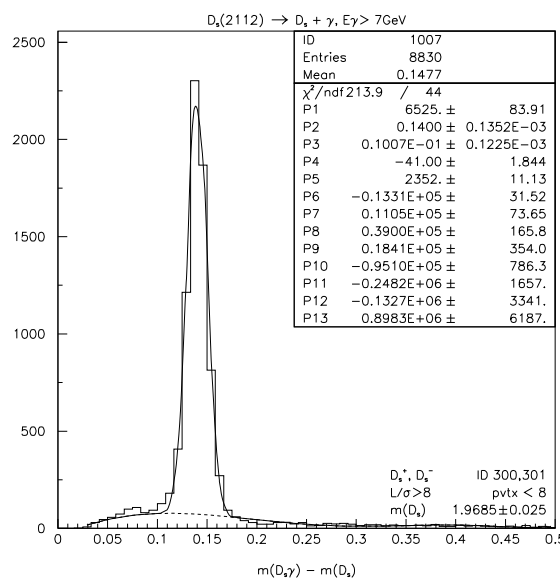


FIG. 48: Monte Carlo: M($K^+K^-\pi\gamma$) - M($K^+K^-\pi$)